**Structural Engineering and Mechanics**, *Vol. 93, No. 3 (2025) 165-179*
https://doi.org/10.12989/sem.2025.93.3.165


# Finite elements investigations of the effect of different parameters on the retrofitted RC beams with anchored FRP plate

Yusuf Sümer*[1], M. Nawar Zakour[1a] and Muhammed Öztemel[2b]

[1]*Department of Civil Engineering, Sakarya University of Applied Sciences, Sakarya, Turkey*
[2]*Graduate Education Institute, Sakarya University of Applied Sciences, Sakarya, Turkey*

(*Received May 5, 2024, Revised January 8, 2025, Accepted January 10, 2025*)

**Abstract.** Fiber-composites constructed of reinforced polymer have recently acquired popularity as an alternative to other traditional materials used in construction reinforcement. These composites are remarkable because of their low weight, high tensile strength compared to its weight ratio, corrosion resistance, and ease of installation in strengthening and retrofitting structural parts. In this work, using the ABAQUS analytical program's finite element algorithm to analyze 279 models, the effects of multiple parameters on the behavior of RC beams externally bonded and retrofitted with one of three types of polymeric fibers were investigated. This was achieved by modeling a quarter of the complete beams using the beams' symmetry, where the cohesive bond model of the FRP-concrete interface and the isotropic elastic characteristics of FRP were applied. Good agreement was found between experimental data and numerical results when the material models were adopted with experimental work. Investigations indicate that a typical collapse happens when the cohesive bond breaks, and that while increasing the shear or concrete strength improves the allowable loading capacity, but it does not completely prevent the debonding failure of the beam. U-wrap anchor applications at the end of external bonding are a partial solution to the problem of early collapse in the more rigid fibers, like carbon fiber polymers. The effect of using U-wrap anchors to reduce early collapse varies depending on the stiffness of the fiber; it is effective in the least rigid fibers, like glass fiber-reinforced polymers, but less effective by increasing the stiffness of the fibers, like aramid fiber-reinforced polymers. Furthermore, increasing the U-wrap anchor width is more effective in eliminating the debonding than increasing its height.

**Keywords:** debonding failure; externally bonded (EB); fiber reinforced polymer (FRP); finite element method (FEM); retrofitted reinforced concrete (RRC)

## 1. Introduction

Due to technical and scientific progress in the world, traditional methods such as concrete jackets and reinforcement with metal plates are no longer the focus of attention among construction companies for many different reasons which were mentioned in some publications (Kachlakev *et al.* 2000, Valivonis *et al.* 2006). Concrete structures may lose their structural integrity due to various factors, including inadequate initial design or construction, lack of maintenance, material degradation, high costs, and design loads, or the need for complex implementation techniques. These structural challenges have been extensively discussed in publications such as those by (Xian *et al.* 2022, Shin *et al.* 2003, Banibayat 2013). The use of fiber-reinforced polymer (FRP) for repairing, retrofitting, or rehabilitating damaged steel and concrete structures is increasingly appealing. This is due to the excellent mechanical properties of FRP, including its high strength and corrosion resistance, as well as its lower maintenance costs and quicker installation times compared to conventional materials. These advantages have been highlighted in subsequent publications (Hollaway 2010, Ammar 2014, Aram *et al.* 2008).

Fiber composites, which are frequently used in civil and structural engineering, are made via pultrusion employing a variety of fiber types, such as aramid fiber (AFRP), glass fiber (GFRP), carbon fiber (CFRP), and basalt fiber (BFRP). GFRP is the most economical among structural FRPs and consequently has the highest consumption rate. Regardless of the direction of fiber orientation, AFRP's low compressive strength makes it less desirable as a structural element. Moreover, high cost of this material and efficient impact absorption makes it the preferred for ballistic-resistant fabrics. Among FRP materials, CFRP boasts the highest strength and the widest range of strengths, which vary depending on the carbon source and manufacturing techniques. In addition, CFRP is more resistant to creep failure than other FRP materials. CFRP is quite expensive, but its remarkable strength and resistance to fatigue and cyclic failures compensate for this. These FRP properties were illustrated by Taerwe Luc (1995). Fig. 1 shows stress-strain curve and comprehensive comparison between behavior of FRP composite materials and steel reinforcements. Some researchers (Wong *et al.* 2023, Qureshi 2022) mentioned that FRP materials also have

*Corresponding author, Associate Professor
E-mail: ysumer@subu.edu.tr
[a]M.D. Student
E-mail: eng.m.nawarzakour@gmail.com
[b]Ph.D. Student
E-mail: d215007002@subu.edu.tr



ISSN: 1225-4568 (Print), 1598-6217 (Online)

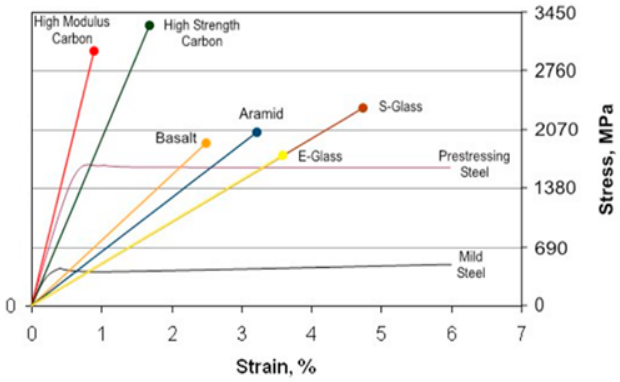


Fig. 1 Comparison of FRP materials with steel

multiple uses in many fields especially in construction work and retrofitting of structural elements. Numerous experimental and analytical investigations have shown that strengthening reinforced concrete (RC) members with fiber-reinforced polymer (FRP) materials via externally from concrete substrate is an excellent way to increase the RC members' load-carrying capability (Teng *et al.* 2003, Al-Negheimish *et al.* 2021, Szewczak 2021).

Despite their positive features, their use still faces challenges, especially when collapsing, as researchers Esfahani *et al.* (2004) have noticed novel failure patterns that potentially impair FRP's performance in retrofit constructions. According to Teng *et al.* (2003), the following is a summary of the typical characteristic failure modes of RC beams (that were flexural strengthened using externally bonded FRP plates):

a) FRP rupture: This occurs when the fibers themselves break or the fiber and resin separate, causing the plate to tear and fail. Although this failure occurs suddenly, it is possible to establish the load levels at fiber rupture more precisely since they are frequently consistent. b) Crushing of compressive concrete: This occurs when the beam bends significantly without the reinforcing bars, FRP plates, or adhesive failing, causing the top of the beam to smash. c) Shear failure: This usually happens when the FRP plate's end is much closer to the support and, as a result, outside of the constant moment zone. There is more shear at this time because the moment is lower. Shear cracks usually start at the plate end and progress to the top of the beam at a sharp diagonal gradient, eventually resulting in abrupt shear failure. d) Concrete cover separation (CCS): This happens when end plate cracks start to appear. Before moving horizontally to a location of high stress, the fractures usually start off traveling diagonally following the alignment of the steel reinforcing bars. Consequently, the concrete cover will rip off and fail. e) Plate end interfacial debonding: This can occur when the concrete or adhesive surface at the beam's face fails. Similar to concrete cover separation, this type of failure occurs when cracks along the beam spread to a high-stress area, but the concrete stays attached to the beam until it is paired with areas where concrete cover separation fails. f) Intermediate flexural crack (IC), is a failure that may be significant when thin FRP plates are used, according to research. A critical flexural crack that forms at the tensile side of the concrete elements is linked to the failure process. Usually, the crack happens in a region with a high bending moment, such the constant moment zone, and failure follows, g) Intermediate flexural-shear crack (IC): similar to the preceding mode, but the failure happens at a location where the crack that started the failure is caused by shear, hence it usually happens at the plate ends. But according to some research (Kalfat *et al.* 2013, Al-Saawani *et al.* 2020), the two most frequent forms of debonding failure modes in FRP-strengthened beams, which are schematically depicted in Fig. 2, are only a small intermediate crack induced debonding (IC debonding) and concrete cover separation failure (CCS) at the plate-end region.

Numerous factors, such as the thickness of the concrete cover, the amount of tension steel bars, the distance between the end of the FRP plate and the beam support, the length, width, thickness, and modulus of elasticity of the FRP plate, the shear span-to-depth ratio, the section geometry, and the concrete strength, are taken into consideration in publications like Al-Saawani *et al.* (2020), Smith *et al.* (2007), Teng *et al.* (2007), El-Sayed *et al.* (2021). These factors can influence the occurrence of a specific debonding failure mode.

In numerical investigations, the finite element (FE) method is a helpful tool for enhancing the simulation of FRP-strengthened beams. Both IC debonding and CCS failures in FRP are intended to be taken into account in recent research such as (Nour *et al.* 2007, Elsanadedy *et al.* 2019, Barour *et al.* 2019). In order to simulate the behavior of FRP-strengthened RC beams, numerous FE models have been created, taking into account various methodologies. In several FE investigations, the response of the reinforced members was simulated using the perfect tie presumption between the concrete layer and FRP. The continuum damage mechanics (CDM) approach and the fracture-energy-based cohesive zone model (CZM) are the two popular modeling techniques. In the CZM technique, the adhesive is represented by interface elements, which can be used to depict delamination and whose behavior is described by a traction-separation rule. In contrast, the CDM technique takes matrix and fiber damage into consideration and is based on the stiffness deterioration of the adhesive parts as enforced by a damage parameter. Both have the capacity to replicate the beginning and development of the debonding failure, according to reports by Reiner (2021), Xu *et al.* (2021).

Because it usually takes place prior to the yielding of tension steel, the plate end (PE) debonding is extremely brittle. Therefore, in order to prevent such a brittle failure and increase the effectiveness of the strengthening EB-FRP system, it is necessary to anchor the EB-FRP reinforcement at its ends (Kalfat *et al.* 2013, Saribiyik *et al.* 2023, Ma *et al.* 2023). In addition, a number of design codes and researchers, including Pham *et al.* (2006), ACI 440.2R-17 (2017), GB-50608 (2010), Concrete Society Design guidance for strengthening concrete structures using fiber composite materials (2012), CNR-DT 200 (2013), take into account guidelines and recommendations when creating and constructing externally bonded fiber-reinforced polymer systems to reinforce concrete structures and lower the chance of debonding. Although there are many

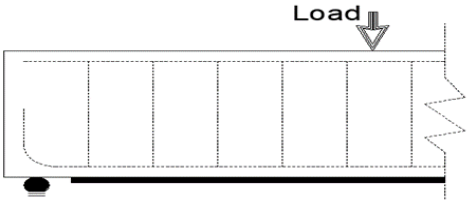


(a) ideal bonding between RC Beam and FRP Plate

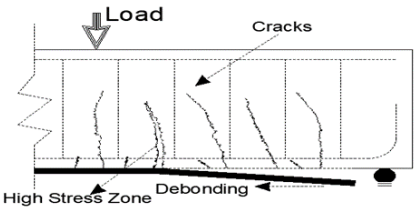


(b) Interfacial debonding caused by intermediate flexural cracks

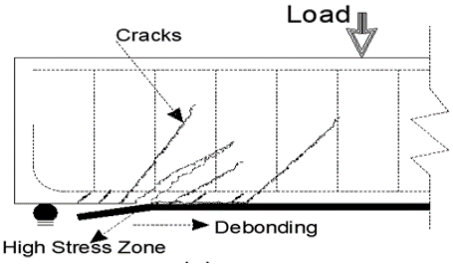


(c) Intermediary flexural-shear cracks causing interfacial debonding

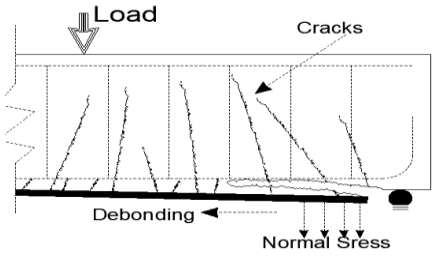


(c) concrete cover detachment

Fig. 2 Typical forms of debonding failures in beams reinforced with FRP

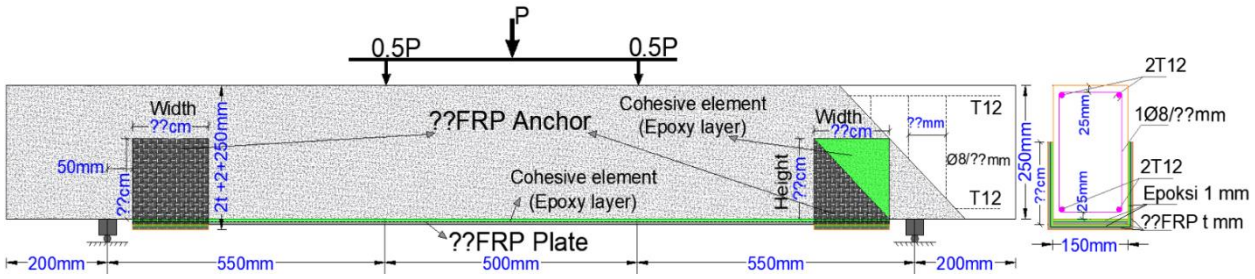


Fig. 3 The geometry, reinforcing placement, and boundary condition of tested beams

strengthening systems to solve the problem of the risk and brittleness of PE debonding the use of retrofitted with U-Wrap anchors at the sides of beam remains preferred for many reasons, among them are the speed of work, ease of implementation, and lack of need for prior drilling in the beam, in addition to durability against corrosion, which is the most important among the other mentioned solutions in researches (Kalfat *et al.* 2013, Pham *et al.* 2006) because of that, many literatures were conducted about it as follows:

Khan and Ayub (2010), investigated the application of U-shaped external anchorage to enhance the performance and shear resistance of RC beams reinforced with CFRP plates that were externally bonded. However, the reported results are insufficient to draw definitive conclusions. They investigated varying end anchorage depths to assess the effectiveness of U-shaped end anchorages. In the region with the highest shear loading, it was discovered that U-shaped anchorages at plate-end strengthened RC beams effectively. However, the load-carrying capacity was unaffected by the end anchorage's depth. Fu *et al.* (2016), investigated the effectiveness of plate-ended U jacket anchors experimentally. They specifically examined how the curvature between the beam axis and the U-jacket affected the failure of concrete cover separation. In this work, ten full-scale FRP-plated RC beams were tested. The results showed that the ductility and load-carrying capability of FRP-plated RC beams were greatly increased by using FRP U-jacketing at the critical plate end, particularly at a tilted angle of 45°.

Yazdani *et al.* (2020), proposed several FRP anchoring systems to address premature CFRP debonding. They also evaluated small concrete beams reinforced with this recently recommended and anchored laminate. Three-point loading was applied to the beams until they failed. Although the laminate was applied quickly, there were some usability problems throughout the limited usage period.

However, mechanical anchoring were unsuccessful for conventional FRP application and only slightly increased CFRP effectiveness. It was discovered that fan anchors did not work with either type of CFRP laminate. The anchors' contribution was affected by the CFRP rupture's location and relative length. An experimental investigation into the use of FRP U-jackets to postpone or avoid debonding failure in RC beams strengthened in flexure using tension face was carried out by Zhang *et al.* (2020).

They evaluated eleven large-scale RC beams, adjusting FRP U-jackets' width and tilt angle, among other characteristics. The investigation revealed that U-jackets effectively delayed or even prevented debonding failure and enhanced the utilization percentage of the tensile strength of NSM strips. The strength and deformation capacity of the test beams were found to be unaffected by the kind of U-jacket material (CFRP or GFRP). For real-world applications, inclined U-jackets are therefore advised.

A mechanically based model was created by Raheem and Rasheed (2021) to determine the shear capability of a FRP U-wrap anchor type. They used full-scale experimental programs and pull-out test findings from the literature on anchored FRP-strengthened RC beams to calibrate and verify the suggested method. In comparison to experimental programs, the investigation showed that the suggested model was reasonably conservative and precise enough. The cumulative performance of reinforced concrete (RC) beams reinforced with two distinct CFRP configurations (plate only; plate with U-wraps) with variable steel reinforcement ratios and stirrup reinforcement was examined by Al-Khafaji *et al.* (2021). They tested five CFRP-RC beams and two RC beams under static short-term bending and five more CFRP-RC beams under 332 days of continuous loading. The transverse and tension faces of the beams were covered with CFRP sheets. The results showed that CFRP U-wrap increased the beams' strength. Nevertheless, the transverse CFRP strip experienced brittle failure as a result of debonding.

In contrast to FRP sheets, Vahidpour *et al.* (2022) examined the structural performance of reinforced concrete RC beam specimens reinforced with 3D-fiberglass. Six RC beams were constructed, reinforced, and tested under 4-point bending machine. One beam was used as a control, and the others were reinforced with glass and carbon polymer materials, 3D-fiberglass and epoxy resin, and 3D-fiberglass and epoxy resin extended to the sidewalls. 3D-fiberglass U-wrap decreased ductility in comparison to specimens reinforced with 3D-fiberglass that were not wrapped. Additionally, the ultimate load was noticeably raised by the 3D-fiberglass U-wrap. The goal of Nguyen *et al.* (2022) and their group was to identify the differences in mechanical behavior between small strengthened beam specimens and real-sized slab specimens. 30 RC beams of 250×400×5300 mm and reinforced with carbon fiber-reinforced polymer sheets were used in a full-size numerical and experimental investigation. The findings showed that, in contrast to the externally bonded technique, the side-bonded technique increased ductility but not load-carrying capability. It was strongly advised to use U-wraps as anchorage systems at the plate ends, regardless of the bonding method used. The tensile strength capability and adhesion performance of BFRP strips fastened to the concrete surface on notched beams using different anchor types were investigated by Ali Saribiyik *et al.* (2023). They came at the conclusion that, whereas bending length had no effect on load-bearing capacity or bending behavior, anchor type did, based on results from experimental and FE model research. When Dong *et al.* (2023) looked into a connection behavior, they discovered that using a single CFRP anchor increased the bond's ultimate load by an average of 52%.

Recent literature lacks investigation into the effect of dimension changes (height, width, or both) of FRP U-wrap anchors on debonding failure in identical EB FRP-plated RC beams. Moreover, reliable design rules for determining the effectiveness of dimension selection of FRP U-wrap are absent. Therefore, this research studied various parameters, such as changing the spacing between stirrups, the type of concrete, and the dimensions of the U-Wrap anchors, which determine the effect of the U-Wrap anchors in the face of the common collapse challenge discussed previously.

Table 1 Data of studied beams parameters

| Concrete compression strength | Stirrup Spacing (mm) | Type of FRP | Height of anchor (mm) | Width of anchor (mm) |
|---|---|---|---|---|
| C10 | 75 | CFRP | 150 | 150 |
| C20 | 150 | AFRP | 200 | 200 |
| C30 | 225 | GFRP | 250 | 250 |

## 2. Details of parameters of modeled RRC beams

Numerous parametric studies were conducted using the suggested simulation technique. In this research, the effect of applying two concentrated forces on RC beams (150×250×2000 $mm^3$), shown in Fig. 3, was studied, according to three grades of concrete strength (C10, C20 and C30), with longitudinal reinforcement as same as area from the top and bottom equaled to 2T12 of the beam section. In addition to that, stirrup has same section area 1Ø8 with variable three spacing values $S$=75 mm, $S$=150 mm and $S$=225 mm, because of that, the collapse of RC beams varies from the effect of flexural to shear failure. The last beams are also bonded externally with FRP plate from the lower interface using the same type of adhesive epoxy (Sika 330). These plates' width equals to the width of the beam. There are three types of polymeric fibers (CFRP, AFRP and GFRP) (Carbon, Aramid and Glass), that have various stiffness. These FRP plate ends (PE) at each one are fixed with a U-Wrap anchor next to the support from the two sides, which has the same shape with variable dimensions. In order to know the effect of changing the dimensions of the anchor in reducing the problem of debonding that occurs in the cohesive element, the attached Table 1 shows the constants and parameters.

Using the commercial finite element software ABAQUS/Explicit a 3D nonlinear FE model is created in this study to simulate the flexural behavior of FRP retrofitted RC beams. To reduce the analysis time in this program, a quarter of the beam is modeled for each model, utilizing the symmetry property. The effect of parameters on the behavior of the RRC beam is studied according to a force-displacement diagram. Finally, the total number of studied models is 279 models, which are obvious attached parameters in the Table 1.

## 3. Material characteristics and constitutive models

This section describes the properties of constituent materials for numerical models.

### *3.1 Concrete behaviour modelling*

ABAQUS's concrete damage plasticity (CDP) model, developed by Hibbitt *et al.* (2000), was used to model concrete behavior. This model takes into account two primary failure mechanisms: tensile cracking and

Table 2 Required parameters for the CDP model

| | |
|---|---|
| $\epsilon$ | 0,1 |
| $\Psi_{(0)}$ | 30 |
| $f_{b0}/f_{c0}$ | 1.1 |
| $K$ | 0.667 |
| $v$ | 0.0001 |

$\epsilon$: Flow potential eccentricity, $\Psi(0)$: Dilation angle, $f_{b0}/f_{c0}$: The ratio of initial equiaxial compressive yield stress to initial uniaxial compressive yield stress, $K$: The ratio of the second stress invariant on the tensile meridian, $v$: Viscosity parameter

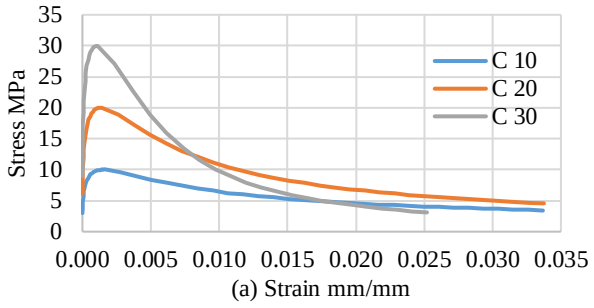


(a) Response of concrete in compression

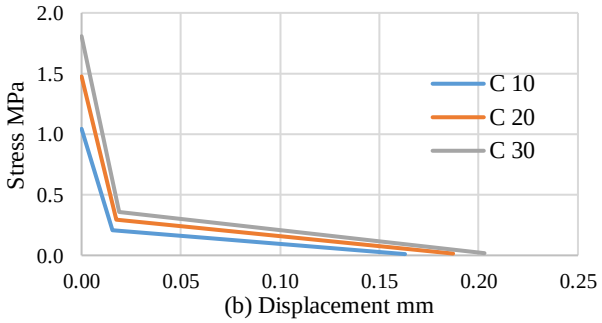


(b) Response of concrete (Bilinear tensile behavior)

Fig. 4 Response of concrete to uniaxial loading

compression crushing. It also calls for five damage parameters, in addition to the modulus of elasticity and Poison's ratio. While the values of other damage parameters are listed in Table 2, the density of concrete is 2,4E-9 ton/m$^3$, and the Poison's ratio is 0.2. A model created by Carreira and Kuang-Han (1986) that is represented in Eqs. (1)-(2)-(3) can be used to model the behavior of concrete under compression by describing the stress-strain curve.

$$f_c = \frac{f_c'\beta\left(\frac{\varepsilon}{\varepsilon_0}\right)}{\beta - 1 + \left(\frac{\varepsilon}{\varepsilon_0}\right)^{\beta}} \quad (1)$$

$$\beta = \frac{1}{1 - \left(\frac{f_c'}{E_0\varepsilon_0}\right)} \quad (2)$$

$$E_0 = \frac{f_c'}{\varepsilon_0}\left(\frac{24.82}{f_c'} + 0.92\right) \quad (3)$$

In this case, $fc$ is the stress that corresponds to the strain ε, and $f_c'$ is the maximum stress, which is the compressive strength. $\varepsilon_0$: the maximal stress-corresponding strain, calculated as 0,0025; $E_0$: the elasticity's initial tangent modulus; $E_c$: Concrete's modulus of elasticity; $G_c$: Concrete's shear modulus of elasticity; The stress-strain diagram's form determines a parameter called $\beta$.

Table 3 Aggregate size-based fracture coefficients

| $d_{max}$ (mm) | 8 | 16 | 32 |
|---|---|---|---|
| $G_{f0}$ (J/m$^2$) | 25 | 30 | 58 |

$d_{max}$ (mm): Max aggregate size, $G_{f0}$ (J/m$^2$): Coefficient

Table 4 Mechanical properties of concrete

| $f'c$ (MPa) | | 10 | 20 | 30 |
|---|---|---|---|---|
| $f_t$ (MPa) | $0,33\times(f'c)^{0,5}$ | 1,044 | 1,476 | 1,807 |
| $E_c$ (MPa) | $4700(f'c)^{0.5}$ | 14862,71 | 21019,04 | 25742,96 |
| $G_c$ (MPa) | $0,5E/(1+v)$ | 6192,79 | 8757,93 | 10726,23 |
| $G_F$ (N/m) | $G_{f0}(f_{cm}/10)^{0,7}$ | 0,025 | 0,0406 | 0,0539 |
| $W_{ch}$ (mm) | $G_F/f_t$ | 0,024 | 0,0275 | 0,0298 |

Eqs. (4) and (5), respectively, were used to calculate the $\varepsilon_0$ and $E_c$ values as suggested by Ahmed (1981), ACI-318 (2008).

$$\varepsilon_0 = (1680 + 7.1f_c') \times 10^{-6} \quad (4)$$

$$E_c = 4700\sqrt{f_c'} \quad (5)$$

Fig. 4(a) shows the entire concrete stress-strain curve under uniaxial compression. Beyond the ultimate stress and into the strain softening phase, the stress-strain curve can be described. Eq. (6) calculates the compressive inelastic strain, which is the total strain less the elastic strain.

$$\tilde{\varepsilon}_{0c}^{in} = \varepsilon - \varepsilon_{0c}^{el} \quad (6)$$

Eq. (7) computes the concrete's tensile strength ($f_t$) in accordance with ACI 318 (2008). In accordance with Coronado and Lopez (2006), the tensile behavior of concrete is considered to be a bilinear model, which is displayed in Fig. 4(b). Eq. (8) calculates the crack opening ($W_{ch}$), which is a ratio of the total external energy ($G_F$) for each unit of area needed to initiate, and completely break a Mode I crack in concrete.

However, according to CEB-FIB (1993), the concrete's Mode I tensile fracture energy is determined by its compressive strength, $f_c'$, as indicated by Eq (9). $G_{f0}$ is a coefficient in this equation that is associated with the maximum aggregate size ($d_{max}$), which in this case is 8 mm. A number of values are provided in Table 3 to use in the computation of mechanical properties, which are provided in Table 4.

Add to that the Fig. 4(b) illustrates the post-peak tensile stiffening behaviour of concrete.

$$f_t = 0.33\sqrt{f_c'} \quad (7)$$

$$G_F = G_{f0}\left(\frac{f'cm}{10}\right)^{0.7} \quad (8)$$

$$W_{ch} = \left(\frac{G_F}{f_t}\right) \quad (9)$$

### *3.2 Steel behaviour modelling*

As illustrated in Fig. 5, the reinforcing steel is modeled

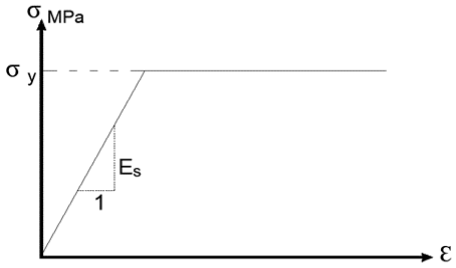


Fig. 5 Stress-strain behavior of reinforcement steel

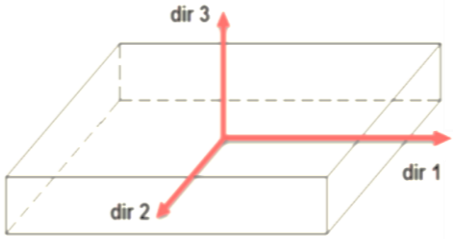


Fig. 6 Reference axes of FRP Strip. (Self-elaboration)

Table 5 FRP elastic properties

| Kind of FRP | CFRP | AFRP | GFRP |
|---|---|---|---|
| ϰs Ton/mm$^3$ | 1,90E-09 | 1,40E-09 | 2,35E-09 |
| *t*, mm | 1,2 | 0,8 | 1,2 |
| $b_f$ mm | 150 | 150 | 150 |
| $E_1$ MPa | 165000 | 120000 | 68000 |
| $E_2$, $E_3$ MPa | 9650 | 6500 | 8200 |
| $Nu_{12}$, $Nu_{13}$ | 0,3 | 0,3 | 0,25 |
| $Nu_{23}$ | 0,45 | 0,34 | 0,3 |
| $G_{12}$, $G_{13}$ MPa | 5200 | 4000 | 4300 |
| $G_{23}$ MPa | 3400 | 3000 | 3600 |

As shown in Fig. 6, $E_1$ and $E_2$ represent the elastic modulus of FRP in directions 1 and 2. On the other hand, the poison's ratio and shear modulus in each direction are represented by $v_{12}$, $G_{12}$, and $G_{23}$.

as elastic-perfectly plastic using the isotropic strain hardening criterion. The material in this model yields when the load is constant. All steel has a modulus of elasticity of 200,000 MPa and a Poisson ratio of 0.3. The yield stress of upper and lower rebars are assumed to be 450 MPa, yield stress of stirrups is assumed to be 355 MPa and the bottom and upper reinforcement area equal to 226.08 mm$^2$.

### *3.3 FRP modelling*

For this purpose, the FRP laminate was modelled as a linear elastic behavior (which means their properties are not same in all directions) up to the brittle failure, where the FRP composite is mainly stressed in the fibre direction. The elastic behavior was modelled as a lamina type in ABAQUS that was authored by Hibbitt and Karlsson *et al.* (2000). The mechanical properties used in the study are presented in Tables 5-6.

### *3.4 Adhesive Interface modelling*

The surface-based interaction attribute is used to model

Table 6 FRP hashin damage model properties

| Kind of FRP | CFRP | AFRP | GFRP |
|---|---|---|---|
| *Xt* MPa | 200 | 1600 | 800 |
| *Xc* MPa | 1600 | 400 | 400 |
| *Yt* MPa | 85 | 65 | 40 |
| *Yc* MPa | 650 | 140 | 110 |
| $S_L$ MPa | 250 | 85 | 60 |
| *ST* MPa | 175 | 85 | 60 |

Tensile and compressive strength of longitudinal ($X_t$, $X_c$), transverse ($Y_t$, $Y_c$) and longitudinal, transverse shear stress ($S_L$, $S_T$) as FRP Hashin Damage Properties.

Table 7 Parameters of bond-slip

| Concrete type | | C10 | C20 | C30 |
|---|---|---|---|---|
| $\beta_w$ | $((2.25\text{-}b_f.b^{-1})/(1.25+b_f.b^{-1}))^{0.5}$ | 0,745 | 0,745 | 0,745 |
| $\tau_{Max}$ MPa | $1.5\beta_w f_{ct}$ | 1,167 | 1,65 | 2,021 |
| $\delta_0$ mm | $0.0195\beta_w f_{ct}$ | 0,0152 | 0,0215 | 0,0263 |
| $K_0$ N/mm$^3$ | $\tau_{Max}/\delta_0$ | 76,923 | 76,923 | 76,923 |
| $G_{cr}$ N/mm | $0.308(\beta_w)^2(f_{ct})^{0.5}$ | 0,1748 | 0,2079 | 0,23 |
| $\delta_f$ mm | $2G_{cr}/\tau_{Max}$ | 0,2996 | 0,252 | 0,2277 |

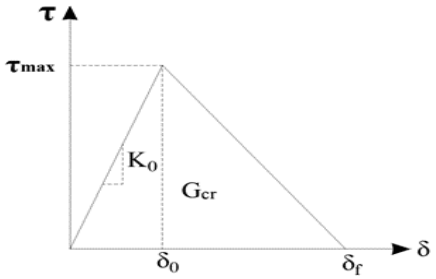


Fig. 7 Bilinear curve for bond-slip

the adhesive. Similar to the cohesive element, the equations and constitution rules of surface-based cohesive behavior call for a linear elastic traction-separation, damage initiation criteria, and damage development law. A bilinear model is used in this study to characterize the constitutive relation of the FRP-concrete interaction. Researchs have shown that this type of model is useful due to its ease of use and ability to accurately forecast interface debonding (Shukri *et al.* 2018, Razaqpur *et al.* 2020). Three factors determine the bilinear traction-separation law, as shown in Fig. 7: starting stiffness ($K_o$), interface shear bond strength ($\tau_{max}$), and fracture energy ($G_{cr}$), which is equal to the area under the traction-displacement curve as provided in Eq. (10)

$$G_{cr} = \frac{\tau_{max}.\delta_f}{2} \quad (10)$$

In this case, $\delta_f$ represents the bond rupture slip at zero interfacial shear stress.

Utilizing the bond-slip interface model put out by Lu *et al.* (2005), the behavior of the FRP-to-concrete contact was modeled. The bond-slip law model equations utilized in this investigation are summed up in Table 7, where *bf* and *b* stand for the FRP laminate and concrete beam widths, respectively, and are depicted in Fig. 8.

The initiation of damage is occurred when a quadratic traction function reaches the value one. This criterion can

Table 8 Mechanical properties of used materials

| | | | |
|---|---|---|---|
| Steel | *Es* | 210 | GPa |
| | *fy* | 507 | MPa |
| | *v* | 0.3 | - |
| Concrete | *f'c* | 30 | MPa |
| CFRP | $E_{CFRP}$ | 165 | GPa |
| | $f_{CFRP}$ | 2 | GPa |

*Es*: Elastic module, *fy*: Yelding stress, *v*: Poisson module, *f'c*: Compression stress, $E_{CFRP}$ : Elastic module, $f_{CFRP}$: yelding stress

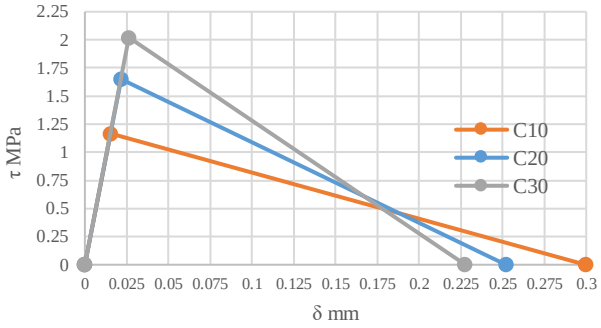


Fig. 8 Bilinear bond-slip curve

be represented in Eq. (11) as follows

$$\left\{\frac{\sigma_n}{\sigma_n^0}\right\}^2 + \left\{\frac{\tau_s}{\tau_s^0}\right\}^2 + \left\{\frac{\tau_t}{\tau_t^0}\right\}^2 = 1 \quad (11)$$

Where $\sigma_n$ is the cohesive tensile strength; $\tau_s$ and $\tau_t$ are shear stresses of the interface; and *n*, *s*, and *t* point to the direction of the stress.

## 4. FEM validation of experiment

### *4.1 Experimental works*

The FEM models covered in the following paragraphs were validated in Obeidat's (2007) study using tested RC beams. Fig. 9 displays the tested beams' geometry, reinforcing placement, and load on a quarter scale. Control beam was loaded up to failure occurred by flexural cracks, *b*. It was strengthened with unidirectional CFRP plate, which was bonded from lower interface by a cohesive element (*Epoxy*), and directed longitudinally to be its length 1560 mm, its width 50 mm, and its thickness 1,2 mm. Furthermore, the beam was loaded until collapse occurred due to flexural cracks as a result of debonding failure, *c*. Control beam was loaded until failure occurred under the influence of shear cracks, *d*. it was retrofitted with vertical strips parallel to the depth of the beam as the same its width and thickness as the previous plates with a height of 300 mm, and an axial spacing between them of 100 mm. It was loaded until collapse occurred under the influence of shear cracks by debonding the vertical plates. Table 8 provides an overview of the material properties as stated by Obaidat (2007).

### *4.2 Numerical analysis*

Table 9 Numerical data of studied models

| Element | Code | Mesh size mm |
|---|---|---|
| Concrete of beam | C3D | 30 |
| Rebar | T3D | 30 |
| FRP | SC8R | 5 |
| Cohesive | COH3D8 | 5 |

C3D: A 4-node linear tetrahedron, T3D: A 2-node linear 3-D truss, SC8R: An 8-node quadrilateral in plane general purpose of continuum shell, finite membrane strains, COH3D8: An 8-node three-dimensional cohesive element.

The finite element approach was used to simulate beams with the same geometry, reinforcement, and loading as in the actual research, Fig. 9. The general-purpose finite element computer program ABAQUS, developed by Hibbitt *et al.* (2000), was used to do the analysis. As seen in Fig. 10, a fourth of the entire specimen was utilized for modeling in order to capitalize on the beam's double symmetry. Fig. 10 shows the boundary conditions. This method greatly decreased the amount of computational time needed. A three-dimensional, eight-node hexahedron solid element was used for structuring the concrete. Two node truss elements were used to represent steel and were embedded in the concrete. Finite membrane strains were taken into consideration in order to depict the behavior of an 8-node quadrilateral general-purpose continuum shell of FRP laminate. For results to be sufficiently accurate, a fine mesh was required. Table 9 listed the mesh density and element type of the verified models.

### *4.3 The result of numerical simulation*

Fig. 11 shows how well the cohesive and FEM models match the experimental findings for the tested beams using previously tested RC beams (Obaidat 2007), which were used to validate the FEM models. This suggests that the constitutive models used for concrete and reinforcement can effectively capture the fracture behavior. Because of the presumed complete bond between the concrete and reinforcement, the FEM analysis predicts that the beam will be slightly stronger and stiffer.

## 5. Results

The models of RC beams were retrofitted at the ends with the U-Wrap anchor technology, according to the numerical data that succeeded in Obaidat (2007) that was mentioned in Table 9 and according to the parameters mentioned in Table 1, to reduce the problem of debonding failure, the improvement in load and deflection was monitored and obtained the following results:

### *5.1 Improvement of load-deflection curve by adding FRP plate and 25×25 anchor*

The RRC beam packages were tested by applying the central load at two known points as in Fig. 3, while changing the spacing of the shear stirrups (str), the type of

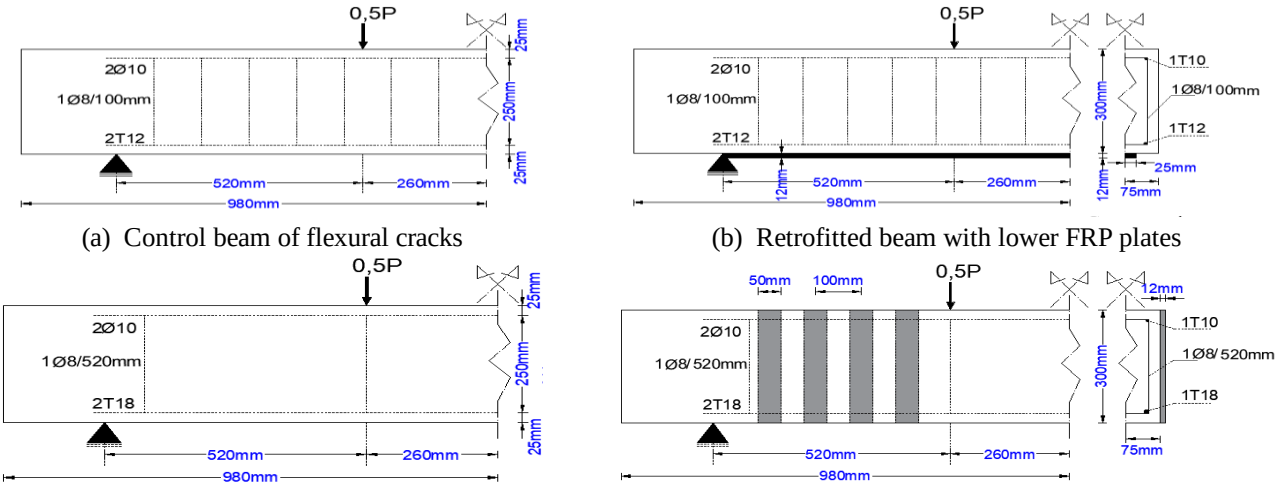


(a) Control beam of flexural cracks (b) Retrofitted beam with lower FRP plates

(c) Control beam of shear cracks (c) Retrofitted beam with vertical FRP strips

Fig. 9 Geometry, arrangement of reinforcement and load by quarter scale of tested beams

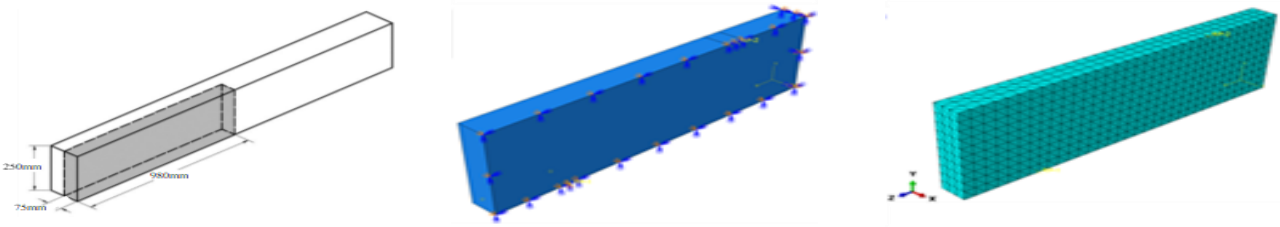

(a) Layout of taking quarter of full beam (b) Boundary conditions of quarter beam (c) Simulating of meshed quarter beam

Fig. 10 Layout of simulated Model in ABAQUS

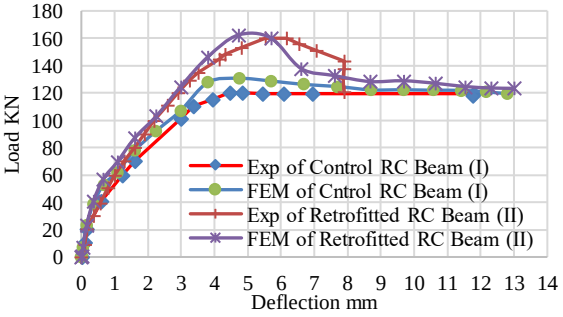


(a) Validation of debonding failure by flexural cracks

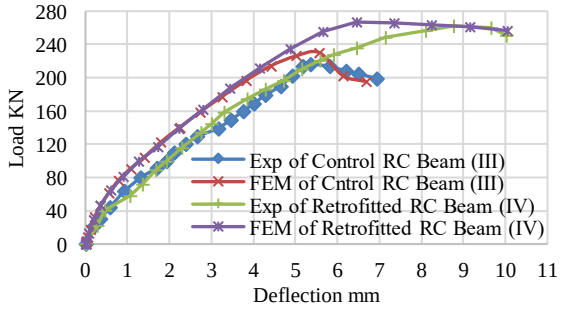


(b) Validation of debonding failure by shear cracks

Fig. 11 Load-deflection curves derived from computational and experimental research

concrete compressive strength (C) and the type of fiber reinforced polymer (FRP) according to data in the Table 1, with one type of U-Wrap anchors with a height of 25 cm and a width of 25 cm (A25×25). It is possible to use abbreviations to facilitate the expression of the model, as the symbol indicates what is changed in it; CB is symbolizing control RC beam, C10 is pointing to concrete with a characteristic compressive stress of 10 MPa, Pl is referring to retrofitted RC beam by FRP plate, Pl&A is pointing to retrofitted RC beam by FRP plate and U-Wrap anchor to both side of beam , Str150 is meaning a spacing between the stirrups is 150 mm, GFRP is referring to a type of fiber reinforced polymer is glass, and A25×20 is pointing to dimension of U-Wrap anchor with a height of 25 cm and a width of 20 cm. A Load-Deflection curves are resulted in Fig. 12.

### *5.2 Calculation of ultimate load according to ISIS and ACI 440-2R Codes and estimate the improvement of RRC beam by FRP Plate & 25×25 anchor*

To know the amount of improvement of the load capacity and the effectiveness of the U-Wrap anchor (A25×25) in reducing the problem of debonding failure, the ultimate moment that the beam can be loaded was calculated by Eqs (12)-(13), which is illustrated in Fig. 13, according to the ACI 440.2R (2017) and Canadian code ISIS (2004) considers a linear strain variation over the depth of sections, and uses the value of 0.0025 for the maximum concrete compressive strain.

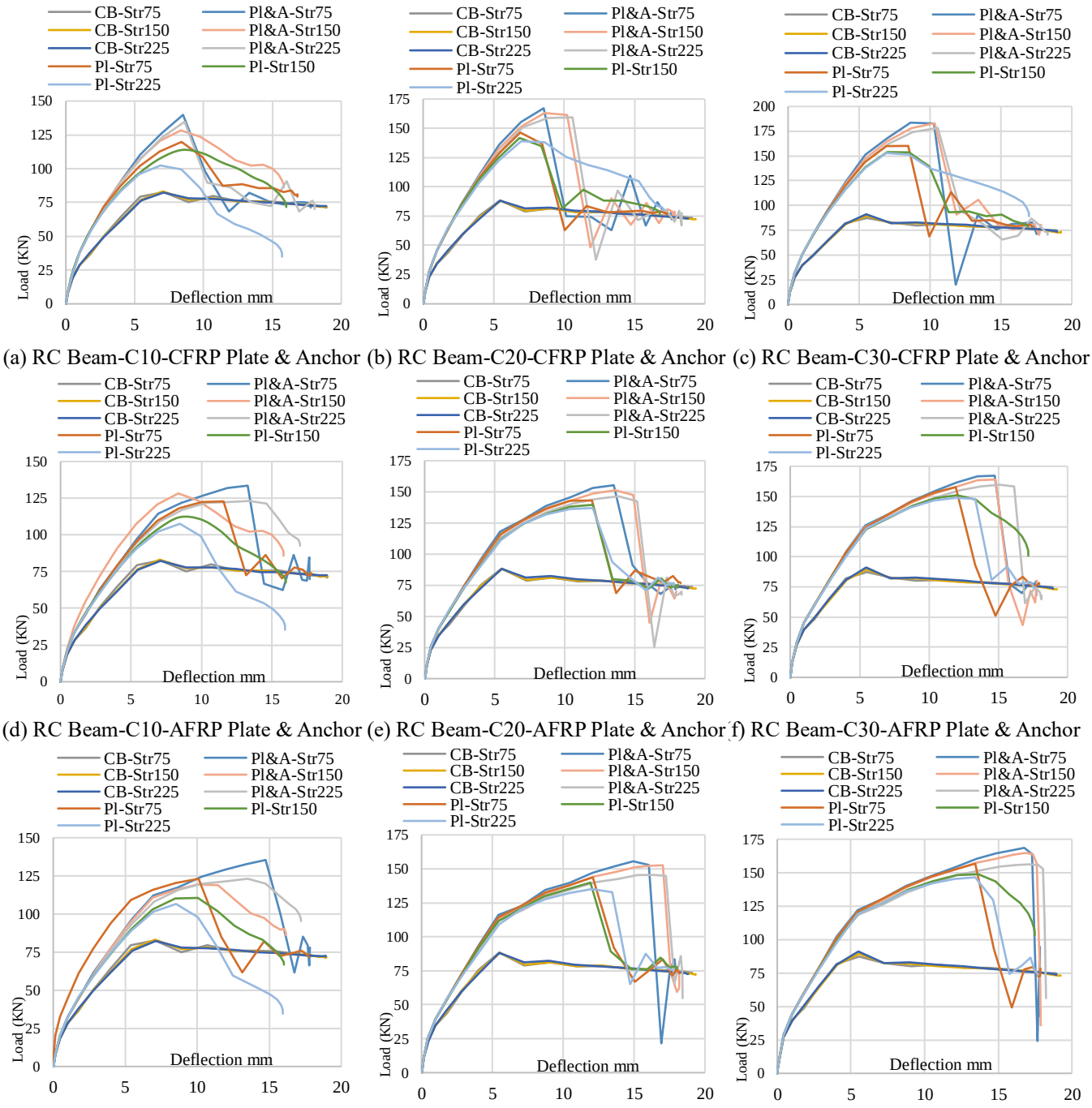


(a) RC Beam-C10-CFRP Plate & Anchor (b) RC Beam-C20-CFRP Plate & Anchor (c) RC Beam-C30-CFRP Plate & Anchor

(d) RC Beam-C10-AFRP Plate & Anchor (e) RC Beam-C20-AFRP Plate & Anchor (f) RC Beam-C30-AFRP Plate & Anchor

(g) RC Beam-C10-GFRP Plate & Anchor (h) RC Beam-C20-GFRP Plate & Anchor (i) RC Beam-C30-GFRP Plate & Anchor

Fig. 12 Load-deflection curves for RRC beam by adding FRP plate and 25×25 anchor

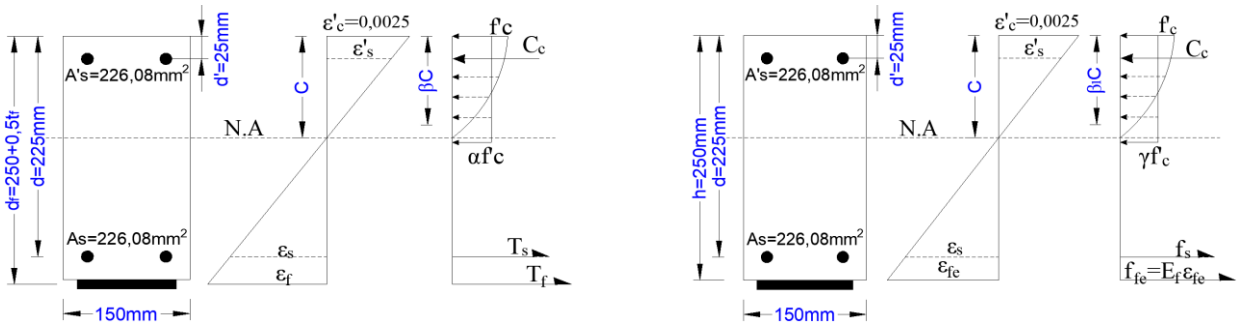


(a) Ultimate moment according to ISIS (b) Ultimate moment according to ACI 440.2R

Fig. 13 Ultimate manual calculated moment

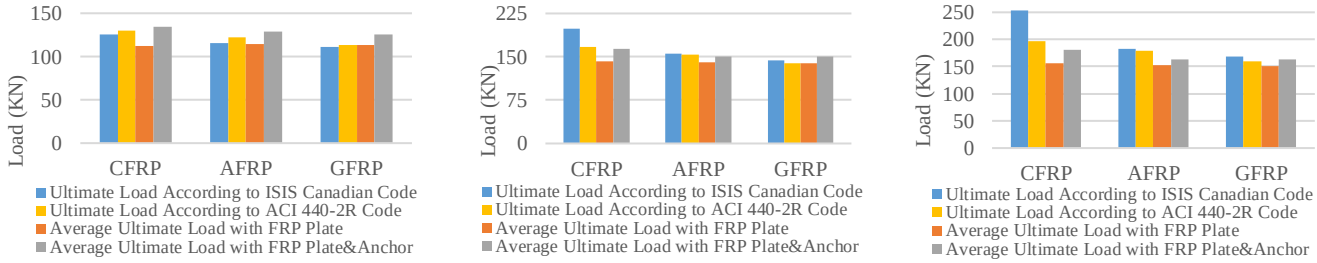


(a) Improvement of load capacity-C10 (b) Improvement of load capacity-C20 (c) Improvement of load capacity-C30

Fig. 14 Improvement of ultimate load of RRC beams

Table 10 Ultimate loads (Units are kN)

| According to | Kind | C10 | C20 | C30 |
|---|---|---|---|---|
| ISIS code | CFRP | 125 | 197,872 | 252,725 |
| | AFRP | 115,683 | 154,632 | 182,933 |
| | GFRP | 111,224 | 144,617 | 168,789 |
| ACI 440-2R code | CFRP | 129,843 | 167,725 | 197,672 |
| | AFRP | 122,258 | 153,901 | 178,663 |
| | GFRP | 113,816 | 139,197 | 158,934 |
| Average ultimate load with FRP Plate | CFRP | 111,985 | 142,345 | 155,690 |
| | AFRP | 114,161 | 139,835 | 152,492 |
| | GFRP | 113,400 | 139,588 | 150,702 |
| Average ultimate load with FRP Plate & Anchor | CFRP | 134,261 | 163,199 | 181,697 |
| | AFRP | 128,338 | 151,048 | 163,629 |
| | GFRP | 125,997 | 151,228 | 163,182 |

Then the ultimate force was calculated after reducing the arm (550 mm) shown according to the Fig. 3 and that is for RRC beam with FRP plate, next to that it was calculated the average ultimate numerical load for stirrup parameters (str 75,150 and 225) in the beam package that is retrofitted only once with a plate and once with a plate and a U-Wrap anchor (A25×25), taking into account the parameters of the FRP and the type of compressive strength of the concrete (C), to produce the values in the Table 10, and this is shown in the Fig. 14, where $M_u$: Ultimate moment, Nmm; $M_n$: Nominal moment, Nmm; $\alpha$, $\beta$: Stress-block factors for concrete, Ø: The reduction factors; $c$: Depth of neutral axis, mm; $A_s$, $A_f$ and $A'_s$ are the areas of the tensile reinforcing bars, FRP sheets and compressive reinforcing bars, respectively, mm$^2$.

Also $\varphi$: The reduction factors' of 0.6, 0.85 and 0.75 for concrete, steel and FRP plate, respectively. $\sigma_s$, $\sigma'_s$, $\sigma_f$ Tensile, compressive strength of steel and tensile strength of FRP Plate, respectively.

$$M_u = \varphi_s A_s \sigma_s \left(d - \frac{\beta c}{2}\right) + \varphi_{frp} A_f \sigma_f \left(d_f - \frac{\beta c}{2}\right) + \varphi_s A'_s \sigma'_s \left(\frac{\beta c}{2} - d'\right) \quad (12)$$

$$M_u = \emptyset \left[A_s \sigma_s \left(d - \frac{\beta_1 c}{2}\right) + \varphi_{frp} A_f \sigma_{fe} \left(h - \frac{\beta_1 c}{2}\right) + A'_s \sigma'_s \left(\frac{\beta_1 c}{2} - d'\right)\right] \quad (13)$$

In Fig. 14 it is clear that the presence of the FRP plate alone does not give close results for moments to that are calculated from equations moment for both past codes, and that adding the U-wrap anchor gives an improvement in the load capacity in all cases because it reduces the problem of debonding failure.

### *5.3 Load capacity ratio in RRC beam by adding FRP plate and 25×25 anchor*

The effect of the load capacity ratio was studied in RC beams by adding an FRP plate to it in case a and observing what happens by adding the FRP plate and anchor together to RC beams in case b, finally to observe the ratio of improvement that occurred in the load capacity the anchor (A25×25) was added to the plated RC beams and to create a visualization of the resulting difference in case c, which can be seen in Fig. 15.

In Fig. 15 it can be noted the load capacity of FRP plates when it added to RC beams which it reaches 80% with some types of FRP in case a, the load capacity in the entire retrofitting schema (plate and anchors), which increases with increased FRP and concrete strength's and reaches 110% with using the CFRP plate in case b, as well as the decrease in the spacing between the stirrups. The load capacity of the U-wrap anchor (A25×25) only can be observed in the case c where its effectiveness is higher with using the CFRP plate and it reaches 32% with some types of FRP.

### *5.4 Deflection capacity ratio by adding FRP plate and 25×25 anchor*

The effect of the deflection capacity ratio was studied in RC beams by adding an FRP plate to it in case a and observing what happens by adding the FRP plate and anchor together to RC beams in case b, finally to observe the ratio of improvement that occurred in the deflection capacity the anchor (A25×25) was added to the plated RC beams and to create a visualization of the resulting difference in case c, which can be seen in Fig. 16.

In Fig. 16 it can be noted the deflection capacity of FRP plates when it added to RC beams which it reaches 150% with some types of FRP in case A, the deflection capacity in the entire retrofitting schema (plate and anchors), which increases with decreasing FRP and concrete strength's and reaches 220% with some types of FRP in case B, as well as the increase in the spacing between the stirrups. The deflection capacity of the U-wrap anchor (A25×25), as can be observed in case C, where its effectiveness reaches 55% with using AFRP or GFRP material as per the RC-plated beam.

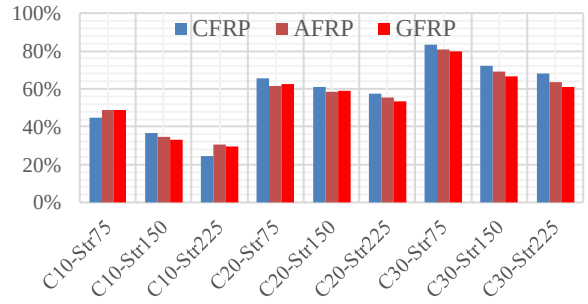


(a) Load capacity ratio of FRP-plate beams as per the RC beam

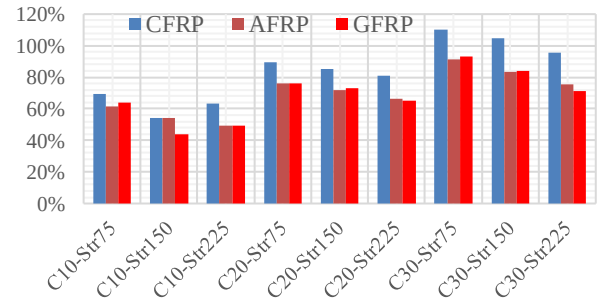


(b) Load capacity ratio of FRP-plate & anchors (A25×25) beams as per the RC beam

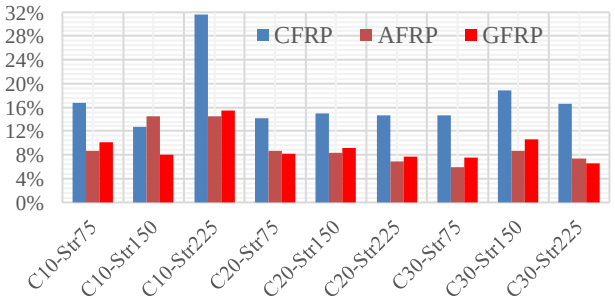


(c) Load capacity ratio of FRP-plate & anchors×(A25×25) beams as per the RC plated beam

Fig. 15 Load capacity improvement ratio of RRC beams with FRP plate & anchors

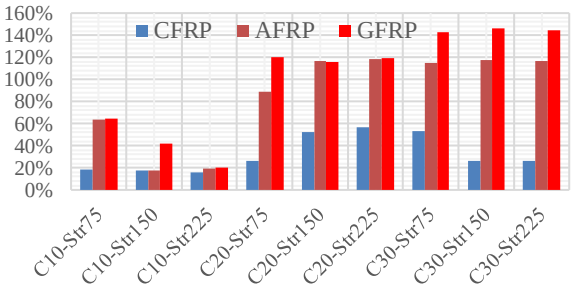


(a) Deflection capacity ratio of FRP-plate beams as per the RC beam

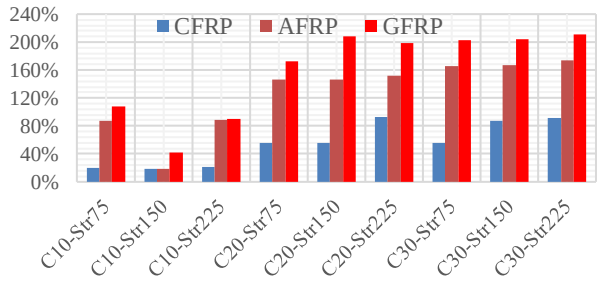


(b) Deflection capacity ratio of FRP-plate & anchors (A25×25) beams as per the RC beam

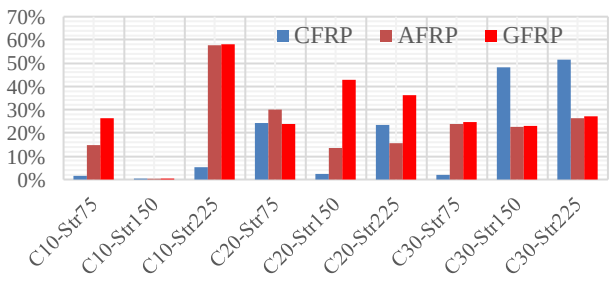


(c) Deflection capacity ratio of FRP-plate & anchors (A25×25) beams as per the RC plated beam

Fig. 16 Deflection capacity improvement ratio of RRC beams with FRP plate & anchors

### *5.5 The effect of dimensions change of U-Wrap anchors in RRC beam with FRP plate and anchor on load capacity ratio*

The effect of increasing the dimensions of the U-Wrap anchors that are added to solve the problem of debonding failure in externally bonded FRP plate on the load capacity ratio was studied as follows: By adopting the standard sample A15×15, the effect of increasing the width only (A15×20, A15×25) was studied, then the effect of increasing the height only (A20×15, A25×15) was also studied, as well as by adopting A20×20 as a standard sample and studying the effect of increasing the width only (A20×25) at once and the effect of increasing the height only at another once (A25×20) and calculating the average load capacity ratio by increasing the width only and the average load capacity ratio by increasing the height only.

In the same way, A15×15 was adopted as a standard sample and the average ratio of load capacity was calculated for increasing the height and width together (A20×20, A25×25) and repeating the matter over the types of FRP in (a) case for CFRP, in (b) case for AFRP and in (c) case for GFRP, so that the results are as shown in Fig. 17.

In Fig. 17 it is clear that the increase in the width of the FRP anchor gives an increase in the capacity of the load, which reaches 6% in the CFRP, and it also appears that the increase in the height leads to a decrease in the load capacity sometimes and leads to an increase of up to 7% in the GFRP. In addition, it is noted that the increase in the height and width together is the most effective, which increases the capacity by up to 14% in the CFRP. The same situation caused an approximately 10% increase in load capacity when GFRP and AFRP were used.

### *5.6 The effect of dimensions change of U-Wrap anchors in RRC beam with FRP plate and anchor on deflection capacity ratio*

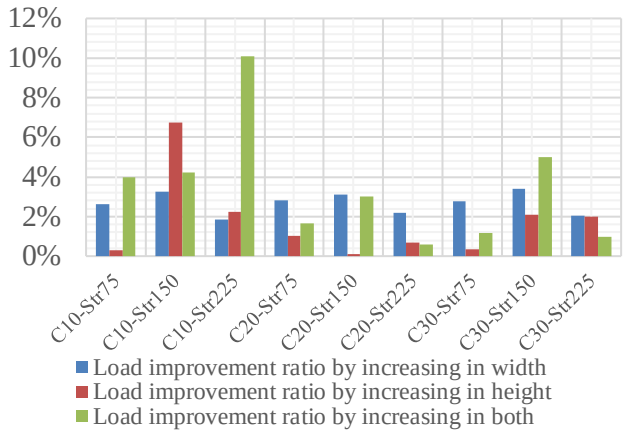


(a) The effect of dimensions change of anchor on load capacity ratio using CFRP type anchor

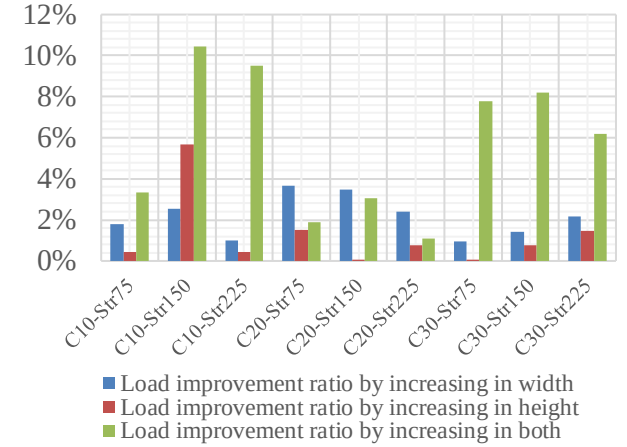


(b) The effect of dimensions change of anchor on load capacity ratio using AFRP type anchor

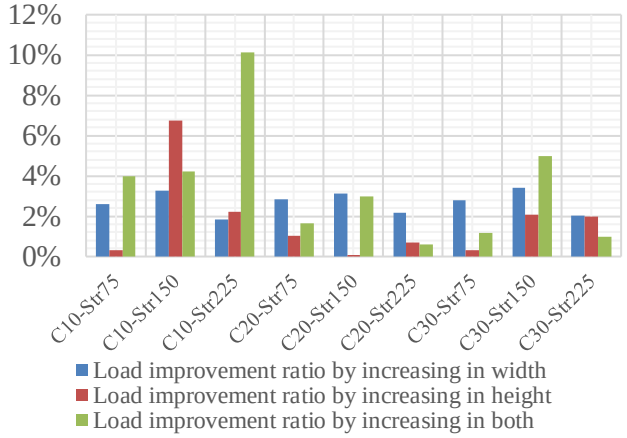


(c) The effect of dimensions change of anchor on load capacity ratio using GFRP type anchor

Fig. 17 Load capacity improvement ratio of RRC beams with change of anchor dimensions

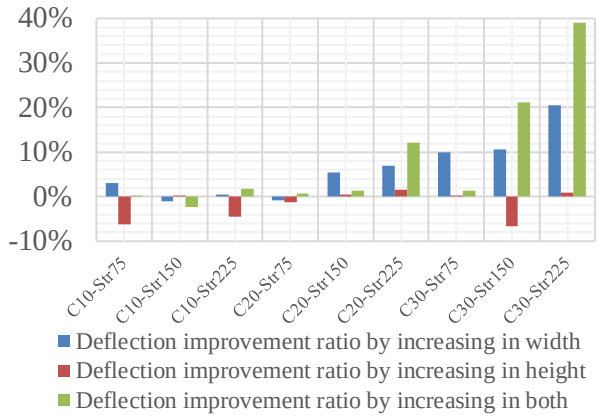


(a) The effect of dimensions change of anchor on deflection capacity ratio using CFRP type anchor

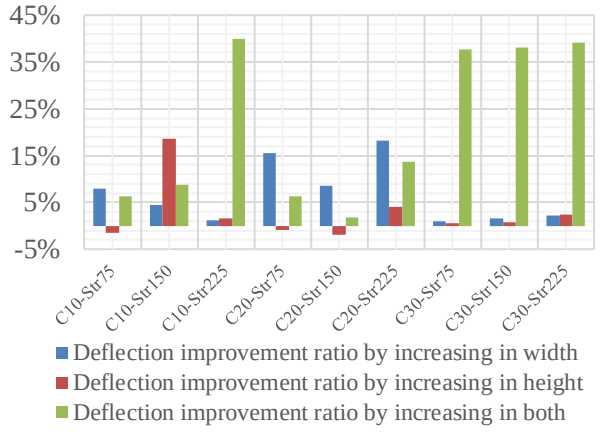


(b) The effect of dimensions change of anchor on deflection capacity ratio using AFRP type anchor

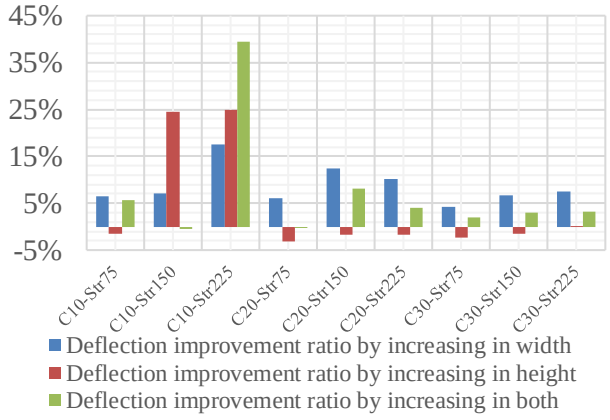


(c) The effect of dimensions change of anchor on deflection capacity ratio using GFRP type anchor

Fig. 18 Deflection capacity improvement ratio of RRC beams with change of anchor dimensions

The effect of increasing the dimensions of the U-Wrap anchors that are added to solve the problem of debonding failure in externally bonded FRP plate on the deflection capacity ratio was studied as follows: By adopting the standard sample A15×15, the effect of increasing the width only (A15×20, A15×25) was studied, then the effect of increasing the height only (A20×15, A25×15) was also studied, as well as by adopting A20×20 as a standard sample and studying the effect of increasing the width only (A20×25) at once and the effect of increasing the height only at another once (A25×20) and calculating the average deflection capacity ratio by increasing the width only and the average deflection capacity ratio by increasing the height only. In the same way, A15×15 was adopted as a

standard sample and the average ratio of deflection capacity was calculated for increasing the height and width together (A20×20, A25×25) and repeating the matter over the types of FRP in (a) case for CFRP, in (b) case for AFRP and in (c) case for GFRP, so that the results are as shown in Fig. 18.

In Fig. 18 it is clear that the increase in the width of the FRP anchor gives an increase in the capacity of the Deflection, which reaches 21% in the CFRP, and it also appears that the increase in the height leads to a decrease in the capacity of the Deflection sometimes and leads to an increase of up to 25% in the GFRP. In addition, it is noted that the increase in the height and width together is the most effective, which increases the capacity by up to 40% in the AFRP. The displacement capacity of the CFRP and AFRP-anchored samples increased with an increase in concrete strength and stirrup spacing, however it decreased with an increase in GFRP-anchored samples.

## 5. Conclusions

After studying tree main types of RC beams: Control beams, externally bonded RC beams with only FRP plate and externally bonded RC beams with FRP plate & U-Wrap anchored whose width, height, or both dimensions were changed, the following results were achieved:

- The load capacity of U-Wrap anchored beams can be increased as the spacing between the stirrups decreases or the compressive strength of the concrete increases.
- It is clear in Fig. 14 that the Canadian code (ISIS) gives higher results for the designed ultimate strength for RRC beams with EB FRP plate than the values given by the American code (ACI 440-2R), especially in CFRP.
- The effectiveness of U-Wrap anchor in reducing the problem of debonding failure increases as the stiffness of the FRP decreases, which is clear in Fig. 14.
- In weak concrete, the effectiveness of the load capacity when adding U-Wrap anchors takes max value when the stirrups spacing is 225 mm because it retrofits the failure of the weak concrete and reduces shear failure. The effectiveness of the load capacity is balanced at all shear stirrup spacing's (75, 150, 225 mm) in C20 concrete, and the effectiveness of the load capacity is greater with the increase in the compression strength of the concrete which is obvious in Fig. 15. The effectiveness of the deflection capacity is inversely proportional to the increase in the stiffness of the FRP, as it takes min value in the CFRP, which was presented in Fig. 16.
- As the width of the U-Wrap anchors increases, the load capacity ratio increases, which is directly proportional to the increase in the compressive strength of the concrete, the increase in the strength of the FRP, and the decrease in the spacing between the stirrups. The load capacity ratio is less than in the previous case when the height of the U-Wrap anchors increases. As shown in Fig. 17, the maximum increase in the ratio of load capacity occurs when the U-Wrap anchors' width and height elevate by the same ratio.
- If the width of the U-Wrap anchors increases, the deflection capacity ratio often increases, which is directly proportional to the decrease in the compressive stress of the concrete and the increase in the spacing between the stirrups. However, at high FRP stiffness, this capacity is directly proportional to the increase in the compressive strength of the concrete. The deflection capacity ratio is often negatively affected, regardless of the stiffness of the FRP when increasing the height of the U-Wrap anchors, and the max increase in the deflection capacity ratio occurs when the width and height of the U-Wrap anchors are increased by the same ratio. In this case, it is directly proportional to the increase in the compressive stress of the concrete, with the exception of FRP, which has low stiffness as it is clear in Fig. 18.
- To understand why both the load and deflection capacity are affected by increasing the height of the U-Wrap anchors, it is recommended to delve deeper into understanding the change in the shear span-to-depth ratio and its effect on the type of debonding failure.

## References

ACI 440.2R-17 (2017) Guide for the Design and Construction of Externally Bonded FRP Systems for Strengthening Concrete Structures, ACI Committee 440, American Concrete Institute, Farmington Hills, MI, USA.

ACI Committee, 3 (2008). Building Code Requirements for Structural Concrete (ACI 318-08) and Commentary. American Concrete Institute, Farmington Hills, MI, 48331, USA.

Ahmad, S.H. (1981), "Properties of confined concrete subjected to static and dynamic loads", Ph.D. Thesis, University of Illinois at Chicago, USA.

Al-Khafaji, A., Salim, H. and El-Sisi, A. (2021), "Behavior of RC beams strengthened with CFRP sheets under sustained loads", *Struct.*, **33**, 4690-4700. https://doi.org/10.1016/j.istruc.2021.07.049.

Al-Negheimish, A.I., El-Sayed, A.K., Al-Saawani, M.A. and Alhozaimy, A.M. (2021), "Effect of stirrups on plate end debonding in reinforced concrete beams strengthened with fiber reinforced polymers", *Polym.*, **13**(19), 3322. https://doi.org/10.3390/polym14091889.

Al-Saawani, M.A., El-Sayed, A.K. and Al-Negheimish, A.I. (2020), "Effect of shear-span/depth ratio on debonding failures of FRP-strengthened RC beams", *J. Build. Eng.*, **32**, 101771. https://doi.org/10.1016/j.jobe.2020.101771.

Ammar, M.A. (2014), "Bond durability of basalt fibre-reinforced polymers (BFRP) bars under freeze-and-thaw conditions", Ph.D. Thesis, Dept. of Civil Engineering, Université Laval, Canada.

Aram, M.R., Czaderski, C. and Motavalli, M. (2008), "Debonding failure modes of flexural FRP-strengthened RC beams", *Compos. Part B: Eng.*, **39**(5), 826-841. https://doi.org/10.1016/j.compositesb.2007.10.006.

Banibayat, P. and Patnaik, A. (2015), "Creep rupture performance of basalt fiber-reinforced polymer bars", *J. Aerosp. Eng.*, **28**(3), 04014074. https://doi.org/10.1061/(ASCE)AS.1943-5525.0000391.

Barour, S., Zergua, A., Bouziadi, F. and Abed Jasim, W. (2020), "Finite element analysis of CFRP-externally strengthened reinforced concrete beams subjected to three-point bending", *World J. Eng.*, **17**(2), 183-202. https://doi.org/10.1108/WJE-04-

2019-01211.
Carreira, D.J. and Kuang-Han, C. (1986), "Stress-strain relationship for reinforced concrete in tension", *ACI Struct. J.*, **83**(3), 21-28.
CEB-FIP MC90 (1993), Comite Euro-International du Beton, CEB-FIP Model Code 1990, Bulletin D'Information, No: 215, Lausanne.
CNR-DT 200 (2013), Guide for the Design and Construction of Externally Bonded FRP Systems for Strengthening Existing Structures Advisory Committee on Technical Regulations for Constructions, National Research Council, Rome, Italy.
Concrete Society Design Guidance for Strengthening Concrete Structures using Fiber Composite Materials, Concrete Society Technical Report No. 55, Crowthorne, UK.
Coronado, C.A. and Lopez, M.M. (2006), "Sensitivity analysis of reinforced concrete beams strengthened with FRP laminates", *Cement Concrete Compos.*, **28**(1), 102-114. https://doi.org/10.1016/j.cemconcomp.2005.07.005.
Dong, K., Gao, Y., Yang, S., Yang, Z. and Jiang, J. (2023), "Experimental investigation and analytical prediction on bond behaviour of CFRP-to-concrete interface with FRP anchors", *Case Stud. Constr. Mater.*, **19**, e02510. https://doi.org/10.1016/j.cscm.2023.e02510.
Elsanadedy, H.M., Al-Salloum, Y.A., Almusallam, T.H., Alshenawy, A.O. and Abbas, H. (2019), "Experimental and numerical study on FRP-upgraded RC beams with large rectangular web openings in shear zones", *Constr. Build. Mater.*, **194**, 322-343. https://doi.org/10.1016/j.conbuildmat.2018.10.238.
El-Sayed, A.K., Al-Saawani, M.A. and Al-Negheimish, A.I. (2021), "Empirical shear based model for predicting plate end debonding in FRP strengthened RC beams", *J. Civil Eng. Manage.*, **27**(2), 117-138. https://doi.org/10.3846/jcem.2021.14304.
Esfahani, M.R., Kianoush, M.R. and Tajari, A.R. (2007), "Flexural behaviour of reinforced concrete beams strengthened by CFRP sheets", *Eng. Struct.*, **29**(10), 2428-2444. https://doi.org/10.1016/j.engstruct.2006.12.008.
Fu, B., Teng, J.G., Chen, J.F., Chen, G.M. and Guo, Y.C. (2017), "Concrete cover separation in FRP-plated RC beams: Mitigation using FRP U-jackets", *J. Compos. Constr.*, **21**(2), 04016077. https://doi.org/10.1061/(ASCE)CC.1943-5614.0000721.
GB-50608 (2010), Technical Code for Infrastructure Application of FRP Composites, China Planning Press, Beijing, China.
Hibbitt, K. and Sorensen, I. (2000), ABAQUS Theory Manual, User Manual and Example Manual, Version 6.7. Providence, Simulia, RI.
Hollaway, L.C. (2010), "A review of the present and future utilisation of FRP composites in the civil infrastructure with reference to their important in-service properties", *Constr. Build. Mater.*, **24**(12), 2419-2445. https://doi.org/10.1016/j.conbuildmat.2010.04.062.
Kachlakev, D. and Mccurry, D.D. (2000), "Behavior of full-scale reinforced concrete beams retrofitted for shear and flexural with FRP laminates", *Compos. J.*, **31**, 445-452. https://doi.org/10.1016/S1359-8368(00)00023-8.
Kalfat, R., Al-Mahaidi, R. and Smith, S.T. (2013), "Anchorage devices used to improve the performance of reinforced concrete beams retrofitted with FRP composites: State-of-the-art review", *J. Compos. Constr.*, **17**(1), 14-33. https://doi.org/10.1061/(ASCE)CC.1943-5614.0000276.
Khalifa, E.S. and Al-tersawy, S.H. (2013), "Experimental and analytical investigation for enhancement of flexural beams using multilayer wraps", *Compos. Part B: Eng.*, **45**(1), 1432-1440. https://doi.org/10.1016/j.compositesb.2012.08.021.
Khan, A.A.R. and Ayub, T. (2011), "Effectiveness of U-shaped CFRP wraps as end anchorages in predominant flexure and shear region", *Advances in FRP Composites in Civil Engineering: Proceedings of the 5th International Conference on FRP Composites in Civil Engineering (CICE 2010)*, Beijing, China, September.
Lu, X.Z., Teng, J.G., Ye, L.P. and Jiang, J.J. (2005), "Bond-slip models for FRP sheets/plates bonded to concrete", *Eng. Struct.*, **27**(6), 920-937. https://doi.org/10.1016/j.engstruct.2005.01.014.
Ma, C., Li, K., Gao, H., Lu, D., Wang, G. and Du, X. (2023), "Seismic performance of underground structures improved by using PET FRP retrofitting central columns", *Tunnel. Undergr. Space Technol.*, **142**, 105435. https://doi.org/10.1016/j.tust.2023.105435.
Module, I.E. (2004), "An introduction to FRP strengthening of concrete structures", Prepared by ISIS Canada, A Canadian Network of Centres of Excellence.
Nguyen, N.T., Nguyen, T.K., Du, D.H., Nguyen, D.N. and Kieu, T.S. (2023), "Nonlinear finite element analysis of FRP-strengthened full-size reinforced concrete beams", *Innov. Infrastr. Solut.*, **8**(5), 139. https://doi.org/10.1007/s41062-023-01110-z.
Nour, A., Massicotte, B., Yildiz, E. and Koval, V. (2007), "Finite element modeling of concrete structures reinforced with internal and external fibre-reinforced polymers", *Can. J. Civil Eng.*, **34**(3), 340-354. https://doi.org/10.1139/L06-140.
Obaidat, Y.T., Heyden, S., Dahlblom, O., Abu-Farsakh, G. and Abdel-Jawad, Y. (2011), "Retrofitting of reinforced concrete beams using composite laminates", *Constr. Build. Mater.*, **25**(2), 591-597. https://doi.org/10.1016/j.conbuildmat.2010.06.082.
Pham, H.B. and Al-Mahaidi, R. (2006), "Prediction models for debonding failure loads of carbon fiber reinforced polymer retrofitted reinforced concrete beams", *J. Compos. Constr.*, **10**(1), 48-59. https://doi.org/10.1061/(ASCE)1090-0268(2006)10:1(48).
Qureshi, J. (2022), "A review of fibre reinforced polymer structures", *Fiber.*, **10**(3), 27. https://doi.org/10.3390/fib10030027.
Raheem, M.M. and Rasheed, H.A. (2021), "Development of an objective model to predict shear capacity of FRP U-wrap anchors", *Compos. Struct.*, **265**, 113762. https://doi.org/10.1016/j.compstruct.2021.113762.
Razaqpur, A.G., Lamberti, M. and Ascione, F. (2020), "A nonlinear semi-analytical model for predicting debonding of FRP laminates from RC beams subjected to uniform or concentrated load", *Constr. Build. Mater.*, **233**, 117838. https://doi.org/10.1016/j.conbuildmat.2019.117838.
Reiner, J. (2021), "A practical approach for the non-local simulation of progressive damage in quasi-isotropic fibre-reinforced composite laminates", *Compos. Struct.*, **265**, 113761. https://doi.org/10.1016/j.compstruct.2021.113761.
Reiner, J., Xu, X., Zobeiry, N., Vaziri, R., Hallett, S.R. and Wisnom, M.R. (2021), "Virtual characterization of nonlocal continuum damage model parameters using a high fidelity finite element model", *Compos. Struct.*, **256**, 113073. https://doi.org/10.1016/j.compstruct.2020.113073.
Saribiyik, A., Al-dhabir, W. and Akbalik, H.H. (2023), "Experimental and FE studies on the bonding performance of basalt FRP bonded to notched concrete beams and improving with anchorage", *Eng. Sci. Technol.*, **46**, 101507. https://doi.org/10.1016/j.jestch.2023.101507.
Shin, Y.S. and Lee, C. (2003), "Flexural behavior of reinforced concrete beams strengthened with carbon fiber-reinforced polymer laminates at different levels of sustaining load", *Struct J.*, **100**(2), 231-239. https://doi.org/10.14359/12487.
Shukri, A.A., Shamsudin, M.F., Ibrahim, Z., Alengaram, U.J. and Hashim, H. (2018), "Simulating intermediate crack debonding

on RC beams strengthened with hybrid methods", *Lat. Am. J. Solid. Struct.*, **15**(9), e78. https://doi.org/10.1590/1679-78254948.

Smith, S.T. and Teng, J.G. (2003), "Shear-bending interaction in debonding failures of FRP-plated RC beams", *Adv. Struct. Eng.*, **6**(3), 183-199. https://doi.org/10.1260/136943303322419214.

Szewczak, A. (2021), "Influence of epoxy glue modification on the adhesion of CFRP tapes to concrete surface", *Mater.*, **14**(21), 6339. https://doi.org/10.3390/ma14216339.

Taerwe, L. (2004), "Non-metallic (FRP) reinforcement for concrete structures", *Proceedings of the Second International RILEM Symposium*, CRC Press.

Teng, J.G., Smith, S.T., Yao, J. and Chen, J.F. (2003), "Intermediate crack-induced debonding in RC beams and slabs", *Constr. Build. Mater.*, **17**(6-7), 447-462. https://doi.org/10.1016/S0950-0618(03)00043-6.

Vahidpour, M., Kheyroddin, A. and Kioumarsi, M. (2022), "Experimental investigation on flexural capacity of reinforced concrete beams strengthened with 3D-fiberglass, CFRP and GFRP", *Int. J. Concrete Struct. Mater.*, **16**(1), 18. https://doi.org/10.1186/s40069-022-00508-w.

Valivonis, J. and Skuturna, T. (2006), "Cracking and strength of reinforced concrete structures in flexure strengthened with carbon fibre laminates", *Civil Eng. Manage. J.*, **13**(4), 317-333. https://doi.org/10.1080/13923730.2007.9636452.

Wong, J., Altassan, A. and Rosen, D.W. (2023), "Additive manufacturing of fiber-reinforced polymer composites: A technical review and status of design methodologies", *Compos. Part B: Eng.*, **255**, 110603. https://doi.org/10.1016/j.compositesb.2023.110603.

Xian, G., Guo, R. and Li, C. (2022), "Combined effects of sustained bending loading, water immersion and fiber hybrid mode on the mechanical properties of carbon/glass fiber reinforced polymer composite", *Compos. Struct.*, **281**, 115060. https://doi.org/10.1016/j.compstruct.2021.115060.

Yao, J. and Teng, J.G. (2007), "Plate end debonding in FRP-plated RC beams—I: Experiments", *Eng. Struct.*, **29**(10), 2457-2471. https://doi.org/10.1016/j.engstruct.2006.11.022.

Yazdani, N., Aljaafreh, T. and Beneberu, E. (2020), "Concrete beam flexural strengthening with anchored pre-saturated CFRP laminates", *Compos. Struct.*, **235**, 111733. https://doi.org/10.1016/j.compstruct.2019.111733.

Zhang, S.S., Ke, Y., Smith, S.T., Zhu, H.P. and Wang, Z.L. (2021), "Effect of FRP U-jackets on the behaviour of RC beams strengthened in flexure with NSM CFRP strips", *Compos. Struct.*, **256**, 113095. https://doi.org/10.1016/j.compstruct.2020.11309.

*CC*